Available online at www.sciencedirect.com
ScienceDirect
Trans. Nonferrous Met. Soc. China 33(2023) 2726−2739
Transactions of Nonferrous Metals Society of China
www.tnmsc.cn

Microstructural role of TiB addition in modifying ZnAl alloy

Yu-lin ZHOU[1,2], Wen-hao SONG[1], Yu-xiang LAI[1], Jiang-hua CHEN[1,3]

1. Center for High-Resolution Electron Microscopy, College of Materials Science and Engineering, Hunan University, Changsha 410082, China;
2. Hunan Nonferrous Metals Holding Group Co., Ltd., Changsha 410015, China;
3. Pico Electron Microscopy Center, Hainan University, Haikou 570228, China

Received 20 July 2022; accepted 24 November 2022

Abstract: The microstructural role of TiB addition in modifying a Zn−Al eutectoid (ZA27) alloy was investigated using scanning electron microscopy, high-angle annular dark-field scanning transmission electron microscopy, and energy X-ray spectroscopy. A series of Zn−27Al−2Cu−0.02Mg−x(Ti+B) (x=0, 0.01, 0.02, 0.05, 0.10, 0.20, wt.%) alloys were cast. The results show that the hardness and strength of the ZA27 alloy are improved with increasing (Ti+B) content, and peak at a (Ti+B) content of 0.05 wt.%. The TiB modifier refines the primary α(Al) phase grains and changes the microstructure of coralloid (α(Al)+η-Zn) eutectoid, which is responsible for the increased mechanical properties of the ZA27 alloy. The modified eutectoid demonstrates featured basket-like and strip-like eutectoid microstructures. The refinement of the primary α(Al) phase grains is very likely related to the constitutional supercooling caused by the segregation of B at the solid−liquid interface. Participation of B and/or Ti in the eutectic and eutectoid reactions modifies the morphology of the eutectoid microstructure.

Key words: Zn−Al alloy; TiB modifier; microstructure; mechanical property; electron microscopy

1 Introduction

Due to the low melting point and good melt flow, zinc alloys are widely used in the manufacture of various die-casting parts and complex-shaped castings [1−3]. In addition, zinc alloys are also widely used as structural and wearing parts due to their excellent mechanical properties, loadbearing capacity, and wear resistance [4−8]. Zn−Al eutectoid (ZA27) alloy is one of the most important zinc alloys and is mainly composed of zinc and aluminum. Among the main grades of zinc−aluminum alloys, ZA27 alloys have the best hardness, strength, and wear resistance [9]. Thus, ZA27 alloys are extensively employed in situations of low to medium speed and high load, serving as wearing parts, such as bearings, bushings, and worm gears, and have become the first choice to replace copper alloys in the relevant fields [10−12]. However, in comparison to other zinc alloys, their intrinsic drawbacks of wide solidification temperature ranges and low eutectic temperatures usually lead to severe microporosity and coarse dendrites in ZA27 alloy casts [13−15]. This microstructure is extremely detrimental to the properties and greatly constrains the applications for ZA27 alloys.

Microalloying is an effective method to improve the properties of ZA27 alloys. For instance, ZHANG et al [16] reported that the addition of Cu element benefited both strength and elongation for ZA27 alloys. Specifically, compared with a Zn−27Al (wt.%) alloy, the tensile strength of a Zn−27Al−2Cu (wt.%) alloy increased from 176 to 243 MPa and its elongation increased from 14% to 80%, which was explained by the fact that the Cu

Corresponding author: Yu-xiang LAI, Tel: +86-15200854384, E-mail: yxlai123@hnu.edu.cn
DOI: 10.1016/S1003-6326(23)66293-4

element effectively modified the distribution and morphology of the (α(Al)+η-Zn) eutectoid microstructure [16]. Moreover, LI et al [17] reported that the addition of Y rare-earth element increased the tensile strength of a Zn−27Al (wt.%) alloy from 398 to 434 MPa. The increase of strength should be attributed to the role of Y element, on the one hand, in modifying the dendritic structure of the as-cast microstructure, and on the other hand, in promoting the formation of a number of fine and dispersive YZn_{12} particles, which strongly pinned dislocations and subgrains. Adding modifiers is another method to improve the properties of ZA27 alloys. CHEN et al [18] fabricated TiB_2-reinforced ZA27-based composites by mixing K_2TiF_6 and KBF_4 halide salts into the molten matrix, and the introduction of TiB_2 phase increased the tensile strength from 385 to 434 MPa [18]. This improvement was explained by the refinement of TiB_2 phase on grains and the Orowan strengthening of TiB_2 phase.

From the above research, Cu element is quite beneficial to the microstructure and properties of ZA27 alloys. Addition of Mg element in ZA27 also plays a role in tuning the properties, while unfavorable Mg−Zn phases may appear with high Mg content (≥0.4 wt.%), and trace addition of Mg would rather reduce the intergranular corrosion susceptibility [16]. In addition, TiB_2 particles or Al−Ti−B master alloys appear to be the most suitable modifiers [19]. Therefore, the TiB-modified Zn−27Al−2Cu−0.02Mg (wt.%) alloys are of great interest for engineering applications. Although the effects of alloying elements and modifiers on ZA27 alloys have been extensively investigated, the microstructure characterization of these research works focuses on the micrometer or even millimeter scale, which greatly limits the understanding of modifying mechanisms for ZA27 alloys.

In the present study, a series of Zn−27Al−2Cu−0.02Mg−x(Ti+B) (x=0, 0.01, 0.02, 0.05, 0.10, 0.20, wt.%) alloys were fabricated via casting and the mechanical properties were tested. It is found that the hardness and strength of ZA27 alloys with the (Ti+B) content of 0.05 wt.% made the best mechanical properties. The microstructures of the ZA27 and ZA27−0.05(Ti+B) alloys were characterized, using atomic-resolution high-angle annular dark-field scanning transmission electron microscopy (HAADF-STEM), scanning electron microscopy (SEM), and energy X-ray spectroscopy (EDS). Our results demonstrated a modifier-induced modification of the morphologies of both the primary α phase and the eutectoid microstructure. In light of the difference between the microstructures before and after modification as well as the nature of the modifier, the impact of the modifier on the microstructure of the ZA27 alloy was discussed.

2 Experimental

The ZA27−x(Ti+B) alloys were melted at 580 °C using a laboratorial well-type furnace, with the raw materials of pure zinc, pure aluminum, Al−50Cu, Al−10Mg, and Al−5Ti−1B (wt.%) master alloys, and then cast in an iron mold (Fig. 1(a)) preheated at 200 °C. The chemical compositions of the alloys were measured using a SPECTROBLUE inductively coupled plasma optical emission spectrometer (Table 1). Vickers hardness was tested

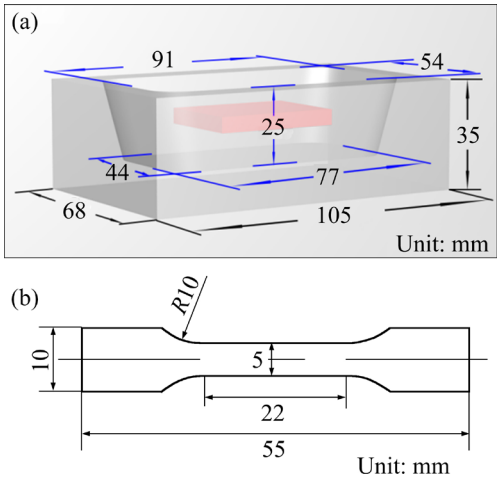

Fig. 1 Illustration of casting mold (a) and tensile sample (b) (The red square in (a) represents the sampling location on the primary ingot)

Table 1 Chemical compositions of ZA27−x(Ti+B) alloys (wt.%)

Al	Cu	Mg	Ti	B	Ti+B	Zn
26.46	2.13	0.01	−	−	0	Bal.
26.60	2.16	0.01	0.008	0.002	0.01	Bal.
26.65	2.11	0.01	0.016	0.003	0.02	Bal.
26.73	2.15	0.01	0.041	0.008	0.05	Bal.
26.57	2.11	0.01	0.081	0.016	0.10	Bal.
26.70	2.16	0.01	0.163	0.032	0.20	Bal.

using an HXD-1000T hardness tester with a load of 500 g and a dwell time of 30 s. Tensile testing was performed at room temperature at a constant strain rate of 5×10^{-4} s^{-1} using an MTS Landmark materials testing machine. Tensile specimens were machined into the dog-bone shape with a gauge size of 2 mm × 5 mm × 22 mm (Fig. 1(b)). Microstructure was characterized using an FEI Quanta 200 SEM equipped with an EDAX Genesis XM−2 EDS detector and an FEI Themis Z scanning/transmission electron microscope (S/TEM) equipped with an FEI Super-X EDS detector. SEM specimens were prepared by mechanical grinding and polishing. STEM specimens were prepared by ion polishing using a Gatan Model 691 precision ion polishing system.

3 Results and discussion

3.1 Mechanical properties

Figure 2 shows the mechanical properties of the as-cast ZA27−x(Ti+B) alloys. The addition of modifier significantly improved the Vickers hardness of ZA27 alloy (Fig. 2(a)). With the increase of (Ti+B) content, the Vickers hardness first increased and then decreased. When the (Ti+B) content was 0.05 wt.%, the Vickers hardness reached a maximum value of HV 184, which was HV 56 higher than that of the alloy without modification. The addition of modifier also remarkably improved the tensile strength of ZA27 alloy (Fig. 2(b)). Like the Vickers hardness, the tensile strength displayed an increasing and then decreasing variation with the (Ti+B) content. The tensile strength of the ZA27−0.05(Ti+B) alloy was the highest and could reach up to 434 MPa, which was 104 MPa higher than that of the unmodified alloy. Nevertheless, the addition of modifier had little effect on the elongation of ZA27 alloy (Fig. 2(c)). The elongations of the ZA27 alloys, which were roughly 4%, were at the same level whether they were modified or not.

Figure 3 shows the morphologies of tensile fracture of the as-cast ZA27 and ZA27−0.05(Ti+B) alloys. The fracture surfaces of the two alloys showed the characteristics of cleavage fracture, that is, a large area of flat facets accompanied by a few tearing ridges. The development of flat facets is known to be correlated with the primary α(Al) dendrites. It should also be noted that the flat facets in the ZA27−0.05(Ti+B) alloy were much smaller than those in the ZA27 alloy, which implies an effective refinement of the as-cast microstructure due to the addition of modifier. The comparable ductility of the unmodified and modified alloys is reflected in their similar fracture modes.

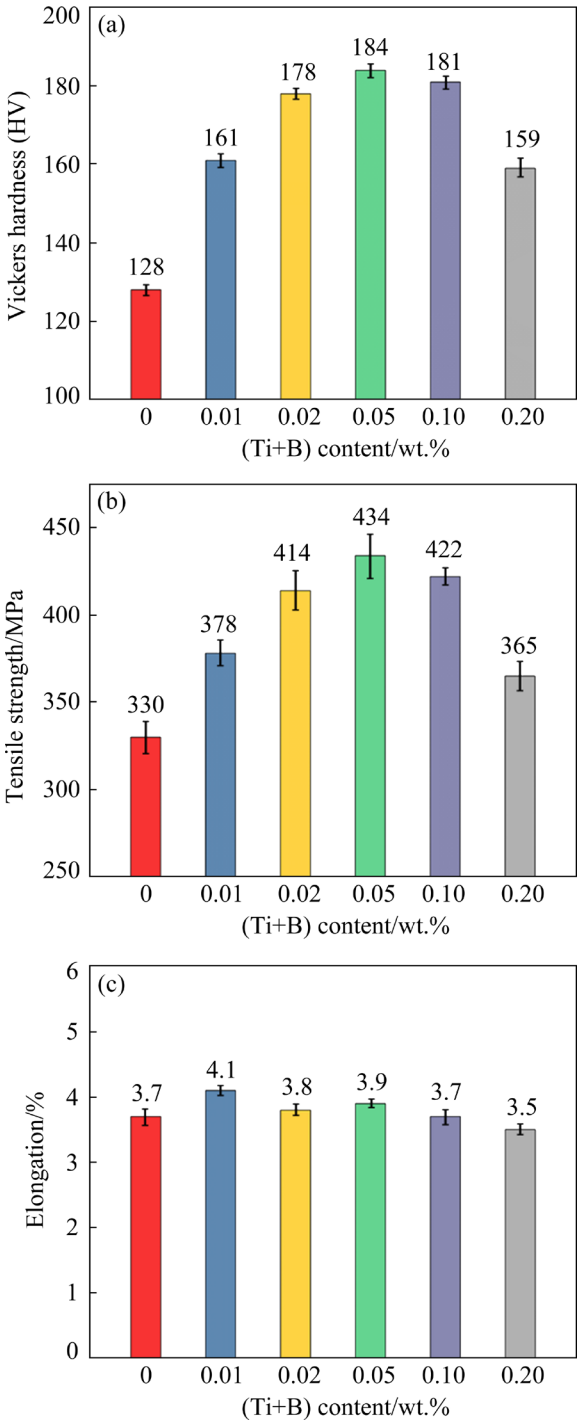

Fig. 2 Vickers hardness (a), tensile strength (b), and elongation (c) of as-cast ZA27−x(Ti+B) (x=0, 0.01, 0.02, 0.05, 0.10, 0.20 wt.%) alloys

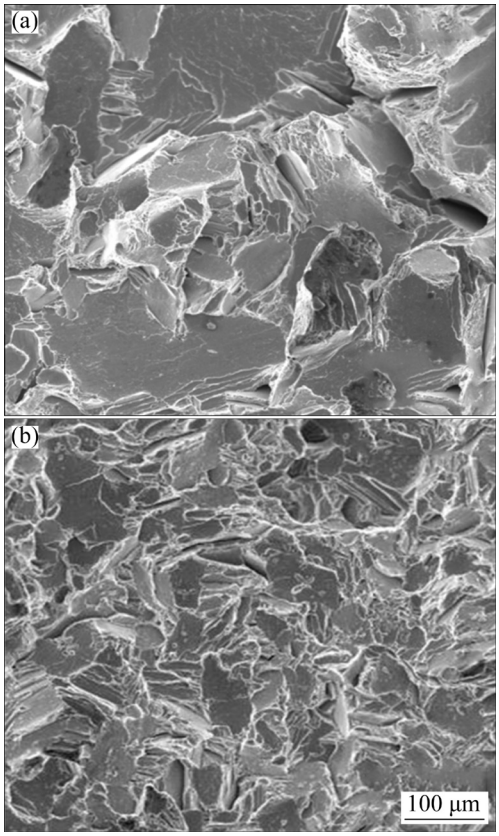

Fig. 3 Fracture surfaces of as-cast ZA27 (a) and ZA27−0.05(Ti+B) (b) alloys

3.2 Microstructure

3.2.1 SEM overviews of microstructure

It is evident from the SEM image of the Al−5Ti−1B master alloy in Fig. 4(a) that this alloy contains particles with blocky and granular morphologies. The blocky and granular particles are identified by their EDS analysis as Al_3Ti and TiB_2, respectively (Figs. 4(b) and (c)). These observations agreed with those in previous work [20].

Figure 5 presents the typical SEM back-scattered electron (BSE) image and EDS point analysis of the ZA27 alloy. There were three distinct types of phases or structures with black, gray, and white contrasts (Fig. 5(a)). The black-contrasted structure constituted the majority of the dendritic structure in the as-cast microstructure; the gray-contrasted structure wrapped around the dendrite arms; the white-contrasted structure filled the gaps in the dendritic structure. The EDS results showed that the black-contrasted structure was enriched with Al, the gray-contrasted structure with Al and Zn, and the white-contrasted structure with Cu and Zn (Figs. 5(b−d)). According to the Al−Cu−Zn ternary phase diagram [21], the black-, gray-, and white-contrasted structures were identified as the primary α(Al) phase, (α(Al)+η-Zn) eutectoid microstructure, and ε-$CuZn_4$ phase, respectively.

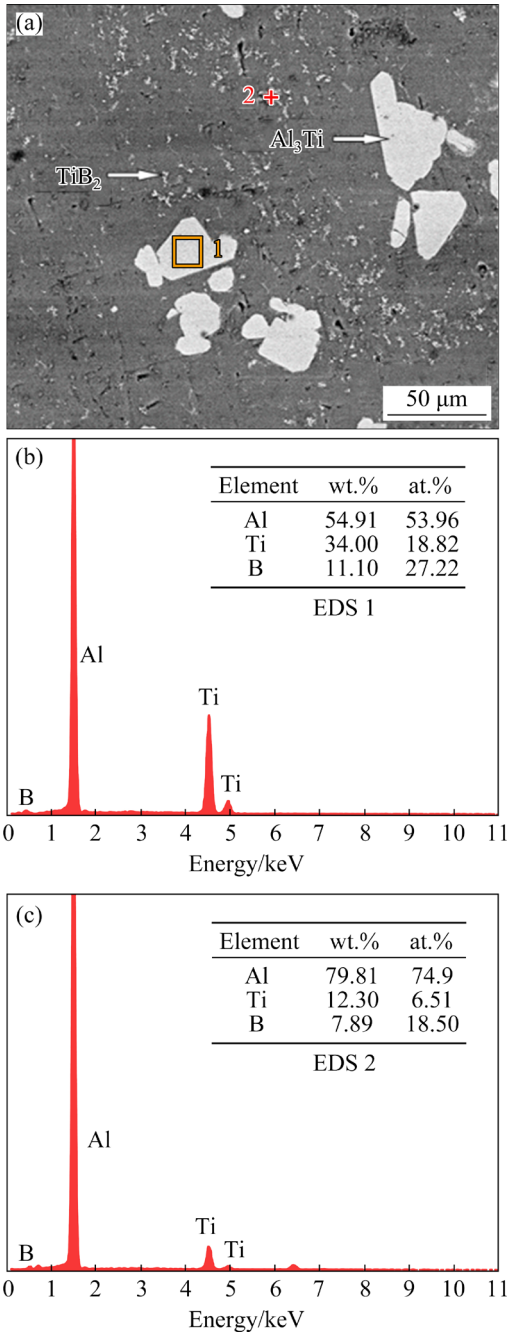

Fig. 4 SEM image (a) and EDS analysis (b, c) of Al−5Ti−1B master alloy

Figure 6 shows the representative low-magnification SEM-BSE image and corresponding EDS mappings of the ZA27−0.05(Ti+B) alloy. Similar to the unmodified alloy, this alloy featured three types of phases or structures with black, gray, and white contrasts (Fig. 6(a)). The average content of each element in the alloy, as determined by EDS

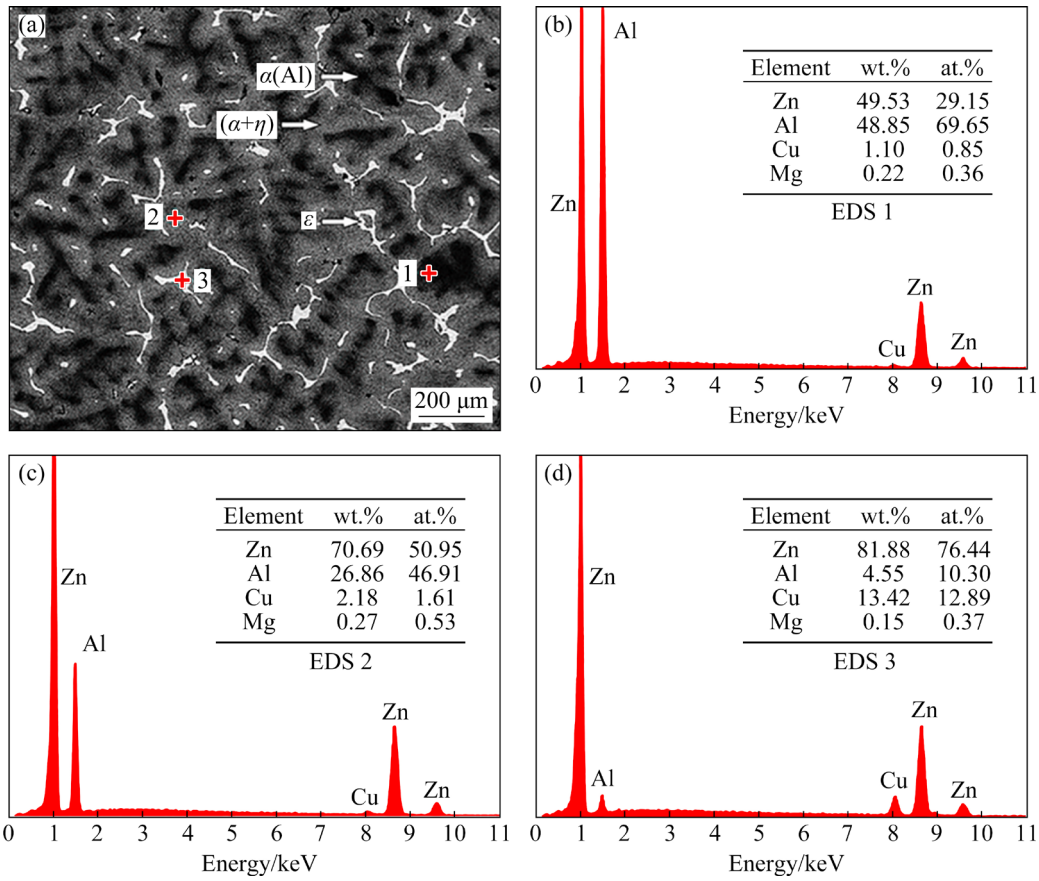

Fig. 5 SEM-BSE image (a) and EDS point analysis (b−d) of as-cast ZA27 alloy

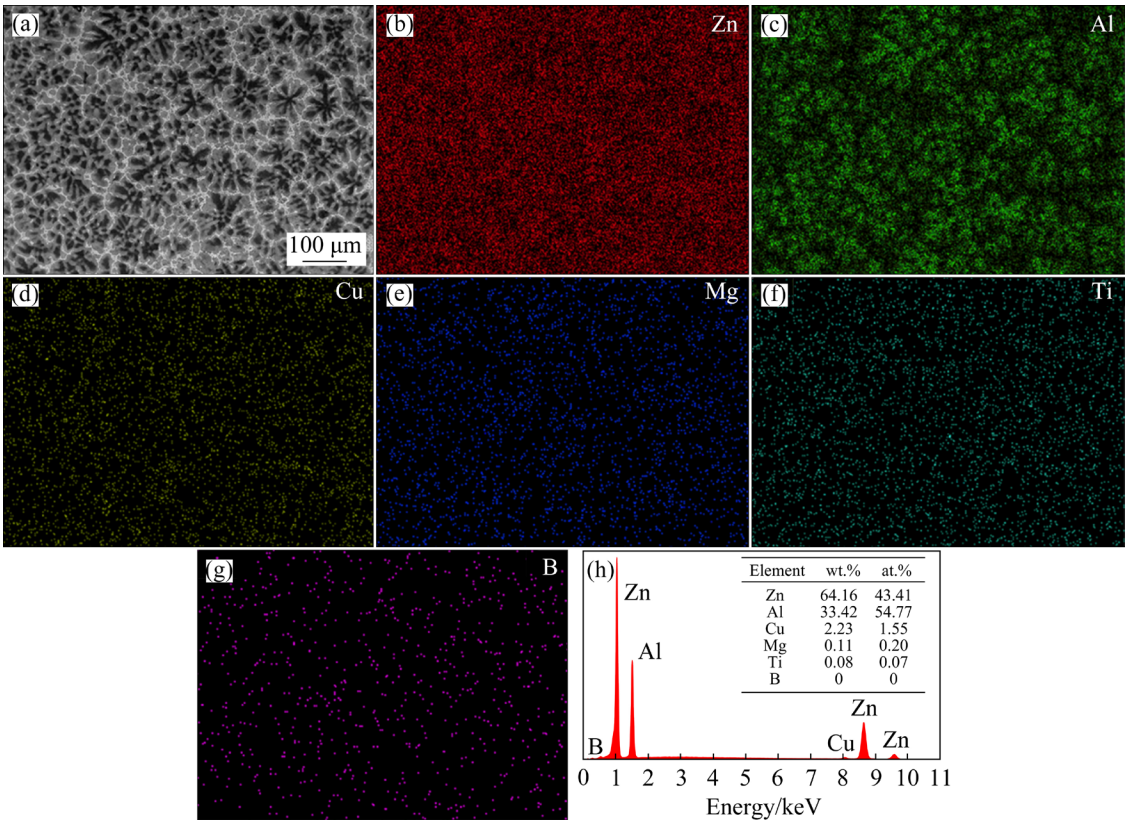

Fig. 6 SEM-BSE image (a) and corresponding EDS mappings (b−g) of as-cast ZA27−0.05(Ti+B) alloy, and EDS results (h) for (a)

(Fig. 6(h)), was close to its nominal content. According to the EDS point analysis (Fig. 7), the black-, gray-, and white-contrasted structures of the ZA27−0.05(Ti+B) alloy were also the primary α(Al) phase, (α(Al)+η-Zn) eutectoid microstructure, and ε-$CuZn_4$ phase, respectively. All three structures contained trace levels of Ti element. Interestingly, compared to the eutectoid microstructure, the primary α-Al and ε-$CuZn_4$ phases had larger B element content. Despite the fact that EDS does not allow for the precise determination of B element, it is still possible to qualitatively evaluate the difference in the contents of these phases. Notably, ZA27−0.05(Ti+B) alloy is the absence of Al_3Ti and TiB_2 particles. This alloy had a low (Ti+B) content, which means that the amounts of Al_3Ti and TiB_2 introduced by the Al−5Ti−1B master alloy were low. Small amounts of these particles are believed to disappear due to melting loss. Comparing the ZA27−0.05(Ti+B) alloy with the ZA27 alloy, the primary α(Al) dendrites in the former alloy were apparently finer than those in the latter alloy. Similar observations for other zinc alloys have been reported in the literature [20,22].

When the (Ti+B) content was increased to 0.2 wt.%, a modest amount of blocky Ti-rich particles were found in the alloy (Fig. 8). These Ti-rich particles primarily contained Al and Ti, with a molar ratio of Al to Ti of almost 3:1, according to the EDS point analysis in Fig. 9. This led to the identification of these particles as Al_3Ti [20]. The Al_3Ti particles either formed during the solidification process or originated from the Al−5Ti−1B master alloy. The average Ti content in the area free of Al_3Ti particles was equal to that in the ZA27−0.05(Ti+B) alloy, both of which were about 0.05 wt.% (Fig. 8(h)). This should be because the Al_3Ti particles had depleted some Ti atoms. The B contents in the primary α(Al) and ε-$CuZn_4$ phase were also higher than that in the eutectoid microstructure (Fig. 10), just like in the case of the addition of 0.05 wt.% (Ti+B).

3.2.2 Morphologies and elemental distributions of eutectoid microstructure

HAADF-STEM characterization on the ZA27 and ZA27−0.05(Ti+B) alloys was carried out to reveal the microstructure of the fine eutectoid microstructure. Low-magnification HAADF-STEM

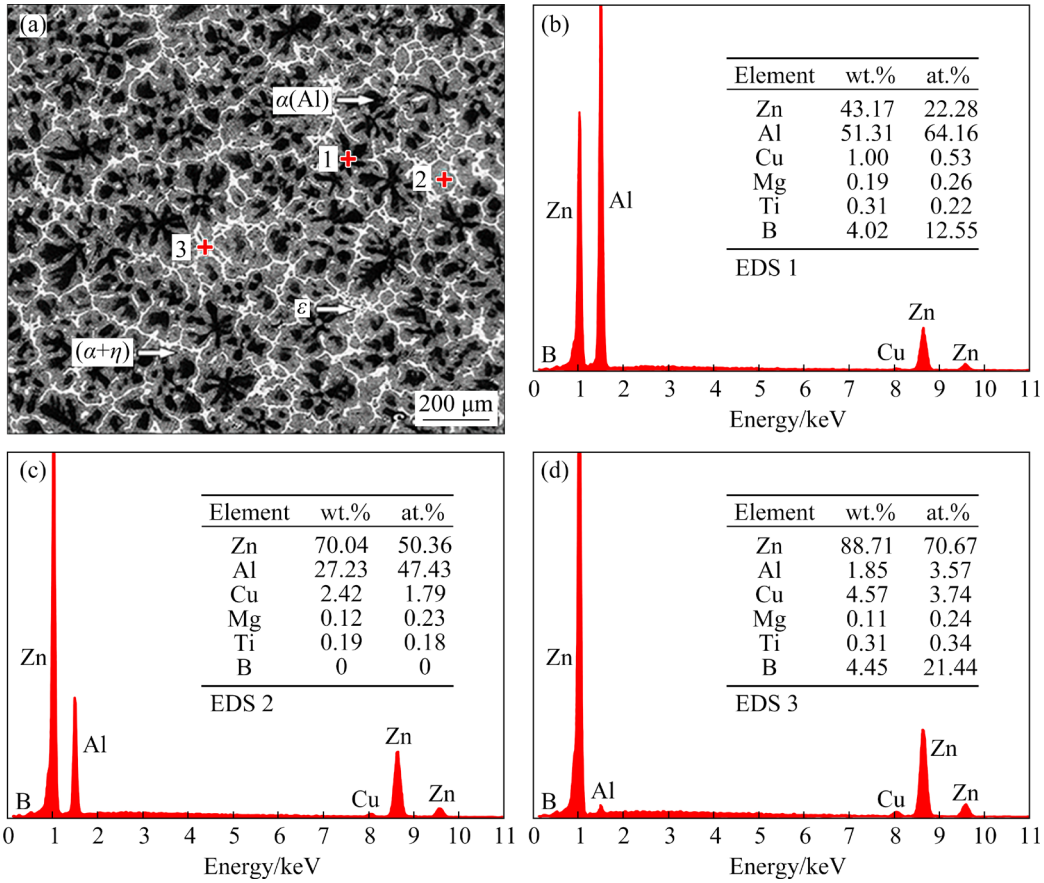

Fig. 7 SEM-BSE image (a) and EDS point analysis (b−d) of as-cast ZA27−0.05(Ti+B) alloy

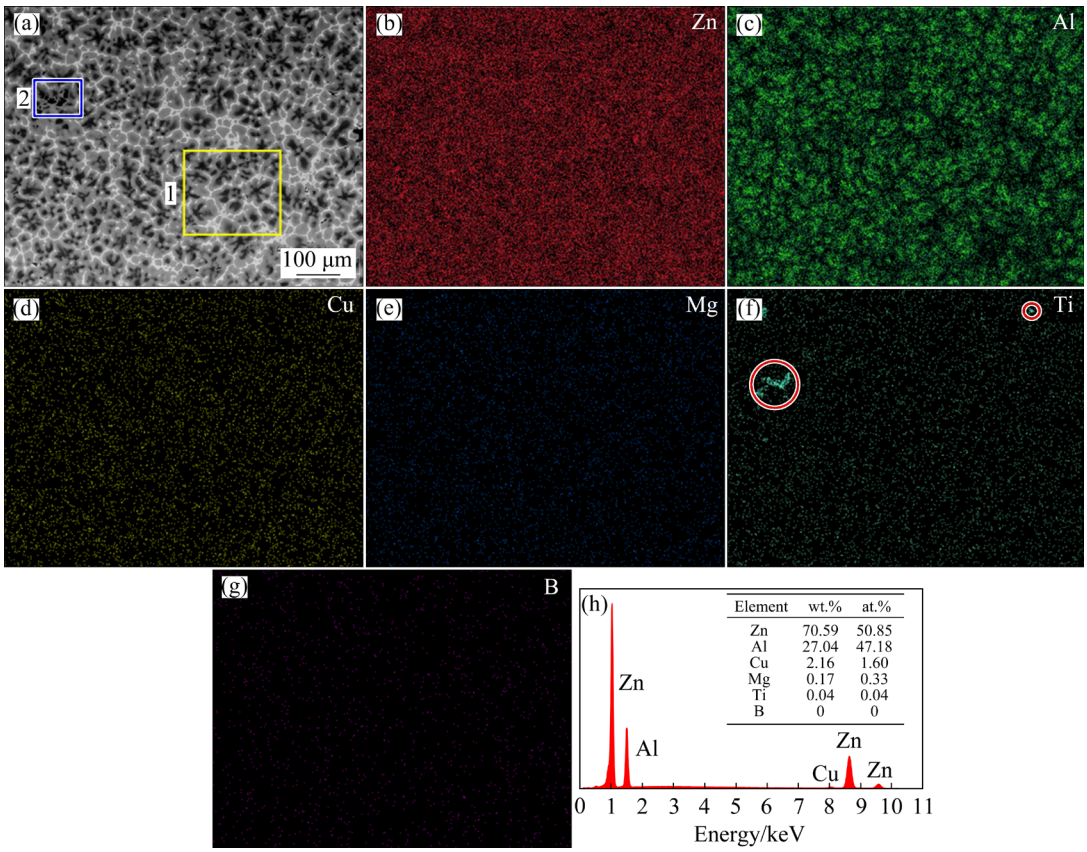

Fig. 8 SEM-BSE image (a) and corresponding EDS mappings (b−g) of as-cast ZA27−0.2(Ti+B) alloy, and EDS results (h) for Region 1 in (a)

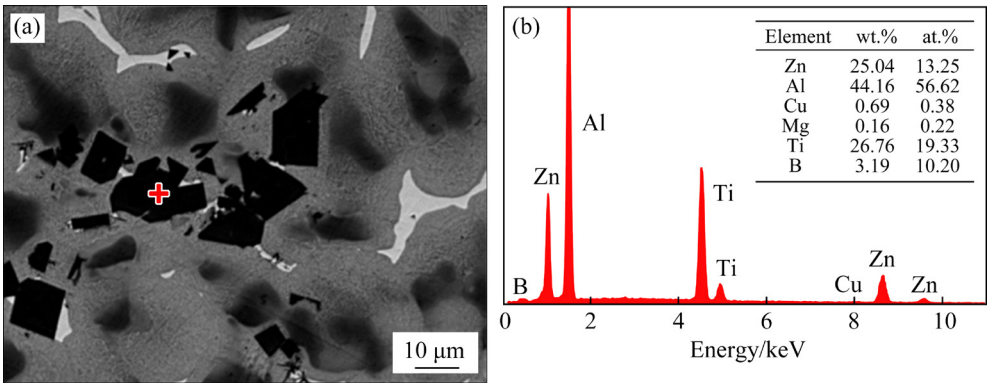

Fig. 9 Enlarged SEM-BSE image (a) and EDS point analysis (b) for Region 2 in Fig. 8(a)

images of the eutectoid microstructures in the two alloys are shown in Fig. 11. The eutectoid microstructure in the ZA27 alloy was composed of coralloid dark-contrasted α(Al) and light-contrasted η-Zn phases (Fig. 11(a)) [16,23−26]. In contrast, the eutectoid microstructure in the ZA27−0.05(Ti+B) alloy was more complicated and displayed three morphologies, marked in Fig. 11(b). The eutectoid microstructure in the Region *A* resembled that of the ZA27 alloy, and the α(Al) and η-Zn phases were coralloid. The eutectoid microstructure in the Region *B* had strip-like α(Al) and η-Zn phases. This type of eutectoid microstructure is comparable to the lamellar eutectoid microstructures that have been identified in other investigations [22]. The strip-like α(Al) and η-Zn phases were longer along their length directions and thinner along their thickness directions as compared to the coralloid ones. In the eutectoid microstructure of the Region *C*, the needle-like and granular η-Zn phases were

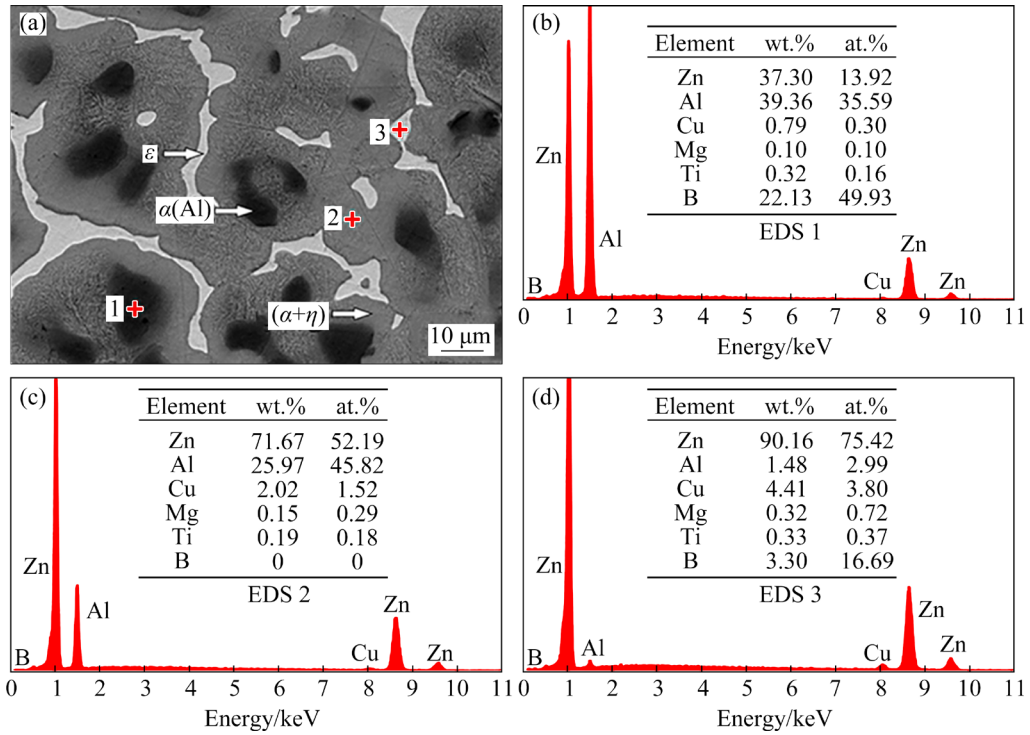

Fig. 10 SEM-BSE image (a) and EDS point analysis (b−d) of as-cast ZA27−0.2(Ti+B) alloy

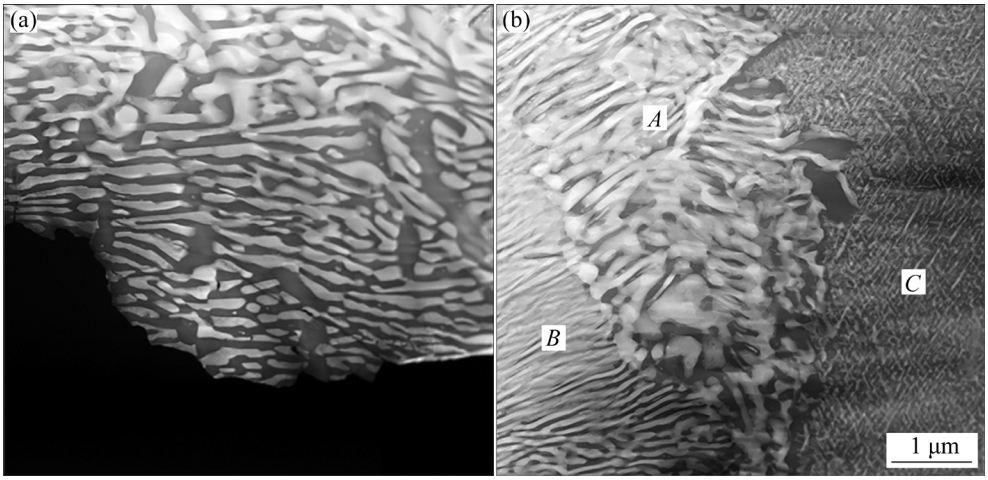

Fig. 11 HAADF-STEM images of eutectoid microstructure in as-cast ZA27 (a) and ZA27−0.05(Ti+B) (b) alloys

connected, and the α(Al) phase was distributed between the η-Zn phases. This type of eutectoid microstructure is referred to as basket-like eutectoid microstructure. A series of HAADF-STEM images revealed that among the three types of eutectoid microstructures, the basket-like type had the highest proportion for the ZA27−0.05(Ti+B) alloy and was the finest in size.

A low-magnification STEM-EDS analysis was performed to investigate the compositions of the three eutectoid microstructures formed in the modified alloy, and the results are displayed in Figs. 12−14. Figure 12 shows the HAADF-STEM image and corresponding EDS mappings of the coralloid eutectoid microstructure. The mappings of Zn and Al elements (Figs. 12(b, c)) and the related EDS data (Figs. 12(h, i)) demonstrate that the bright-contrasted and dark-contrasted phases were the Zn-rich η-Zn and Al-rich α(Al) phases, respectively. Cu and B elements were seen in both the η-Zn and α(Al) phases, but Cu was more concentrated in the η-Zn phase (Fig. 12(d)). In addition, both the η-Zn and α(Al) phases contained trace amounts of Mg and Ti elements.

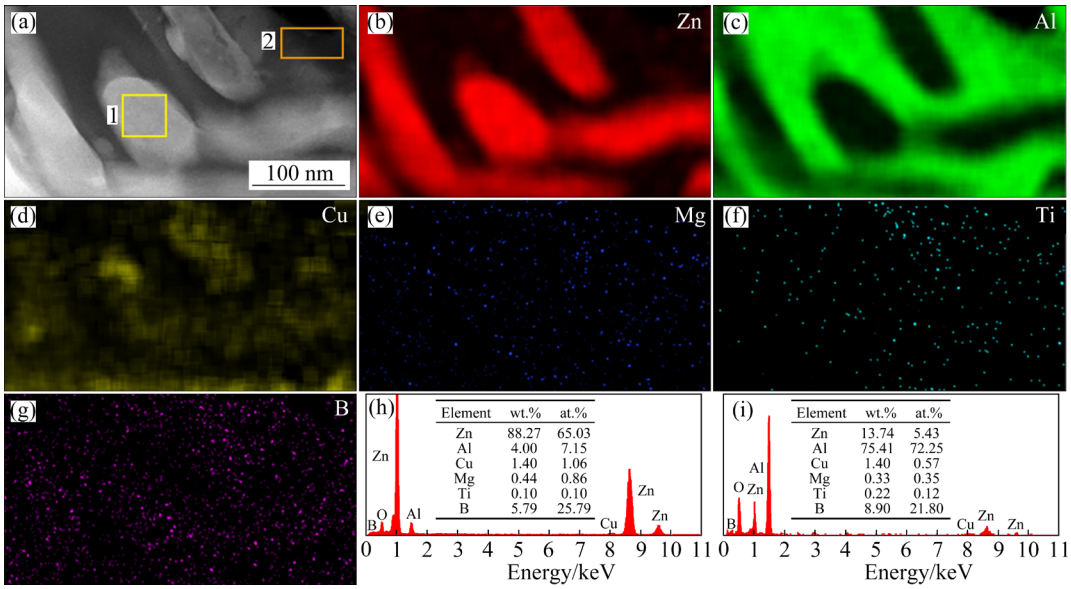

Fig. 12 HAADF-STEM image (a) and corresponding EDS mappings (b−g) of coralloid eutectoid microstructure in as-cast ZA27−0.05(Ti+B) alloy, and EDS results for Region 1 (h) and Region 2 (i) in (a)

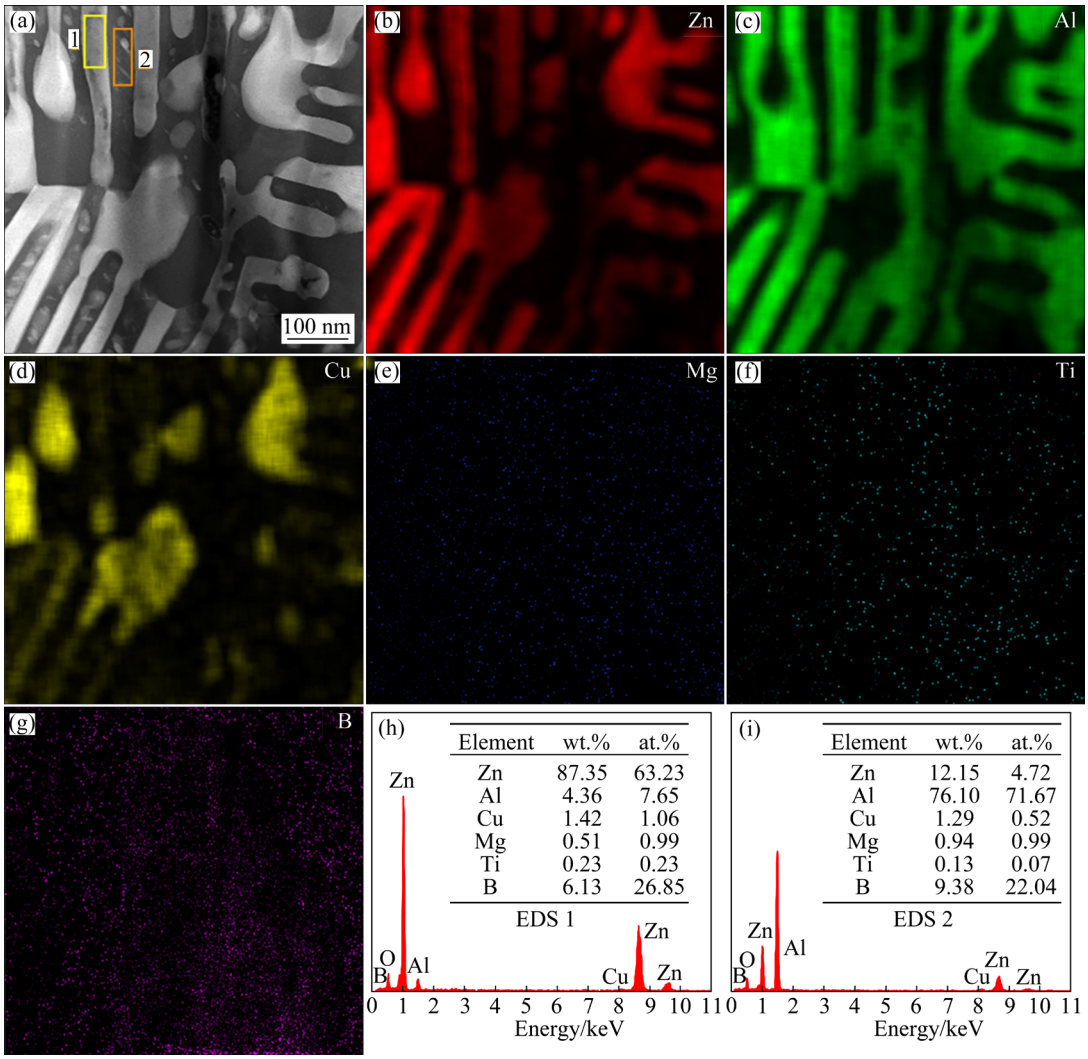

Fig. 13 HAADF-STEM image (a) and corresponding EDS mappings (b−g) of strip-like eutectoid microstructure in as-cast ZA27−0.05(Ti+B) alloy, and EDS results for Region 1 (h) and Region 2 (i) in (a)

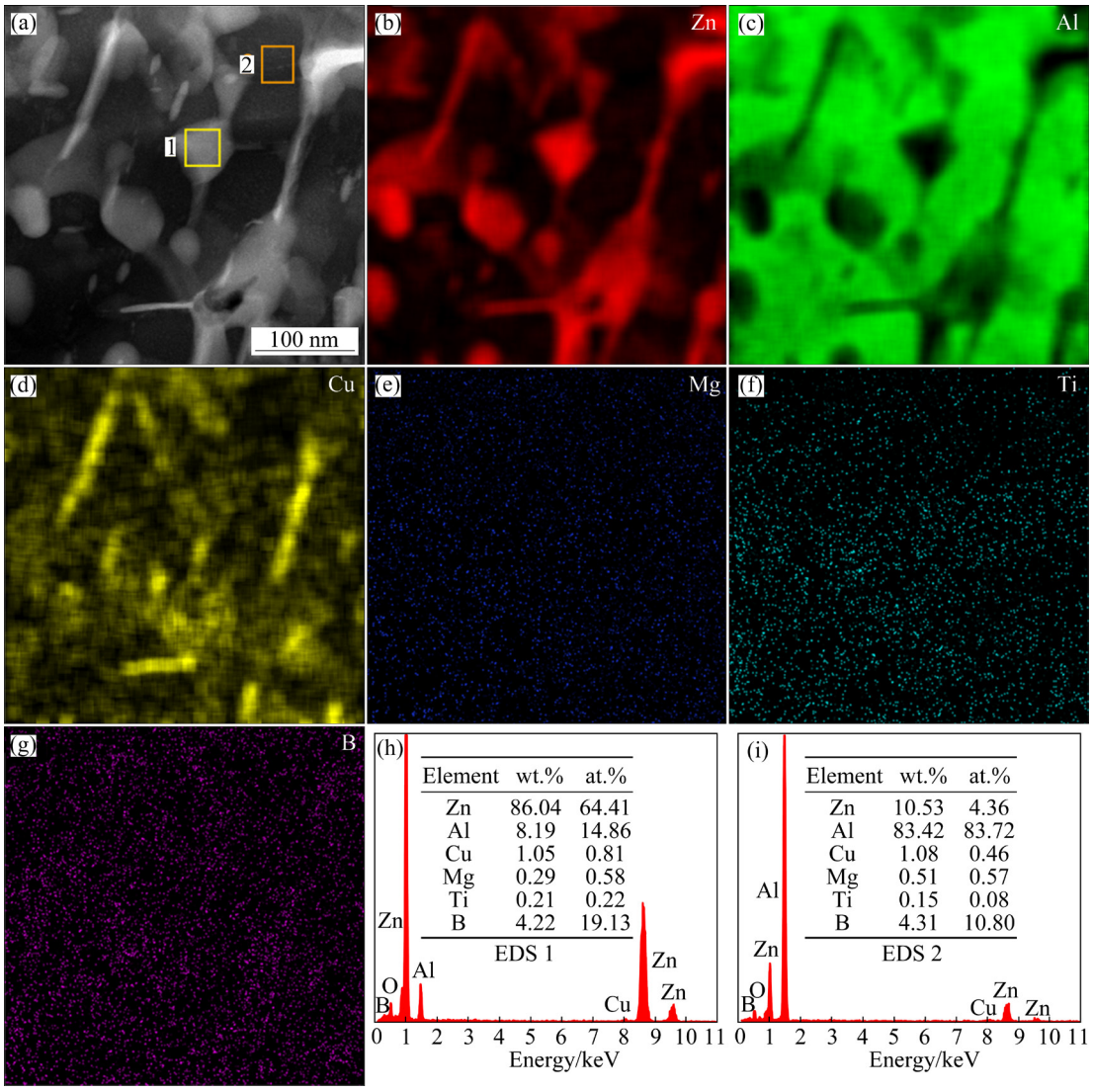

Fig. 14 HAADF-STEM image (a) and corresponding EDS mappings (b−g) of basket-like eutectoid microstructure in as-cast ZA27−0.05(Ti+B) alloy, and EDS results for Region 1 (h) and Region 2 (i) in (a)

The η-Zn and α(Al) phases of the strip-like eutectoid microstructure also mainly contained Zn, Al, Cu, and B, according to the EDS data (Fig. 13). Interestingly, Cu element appeared to be enriched close to the ends of the η-Zn phase strips (Fig. 13(d)). In this kind of eutectoid microstructure, Mg and Ti elements were also present at trace levels.

From the magnified image in Fig. 14(a), the basket-like eutectoid microstructure had a much higher proportion of the α(Al) phase in addition to being finer than the other two types of eutectoid microstructures. Furthermore, compared to the η-Zn phase, the α(Al) phase is more effective at strengthening [27]. As a result, of the three eutectoid microstructures, the basket-like one is believed to contribute most to strengthening. The basket-like eutectoid microstructure was mostly composed of Zn, Al, Cu, and B elements, with traces of Mg and Ti elements, just like the other two eutectoid microstructures (Figs. 14(b−i)). It is intriguing that the needle-like η-Zn phase appeared to have a higher enrichment of Cu element (Fig. 14(d)).

To further confirm the existence of B and Ti in the eutectoid microstructures in the modified alloy, STEM-EDS analysis at the atomic scale of the η-Zn phase of these eutectoid microstructures was conducted, as shown in Fig. 15. The Zn distribution in Fig. 15(b) corresponded well to the Zn atomic-columns in Fig. 15(a), indicating an atomic-resolution EDS analysis. The η-Zn phase contained

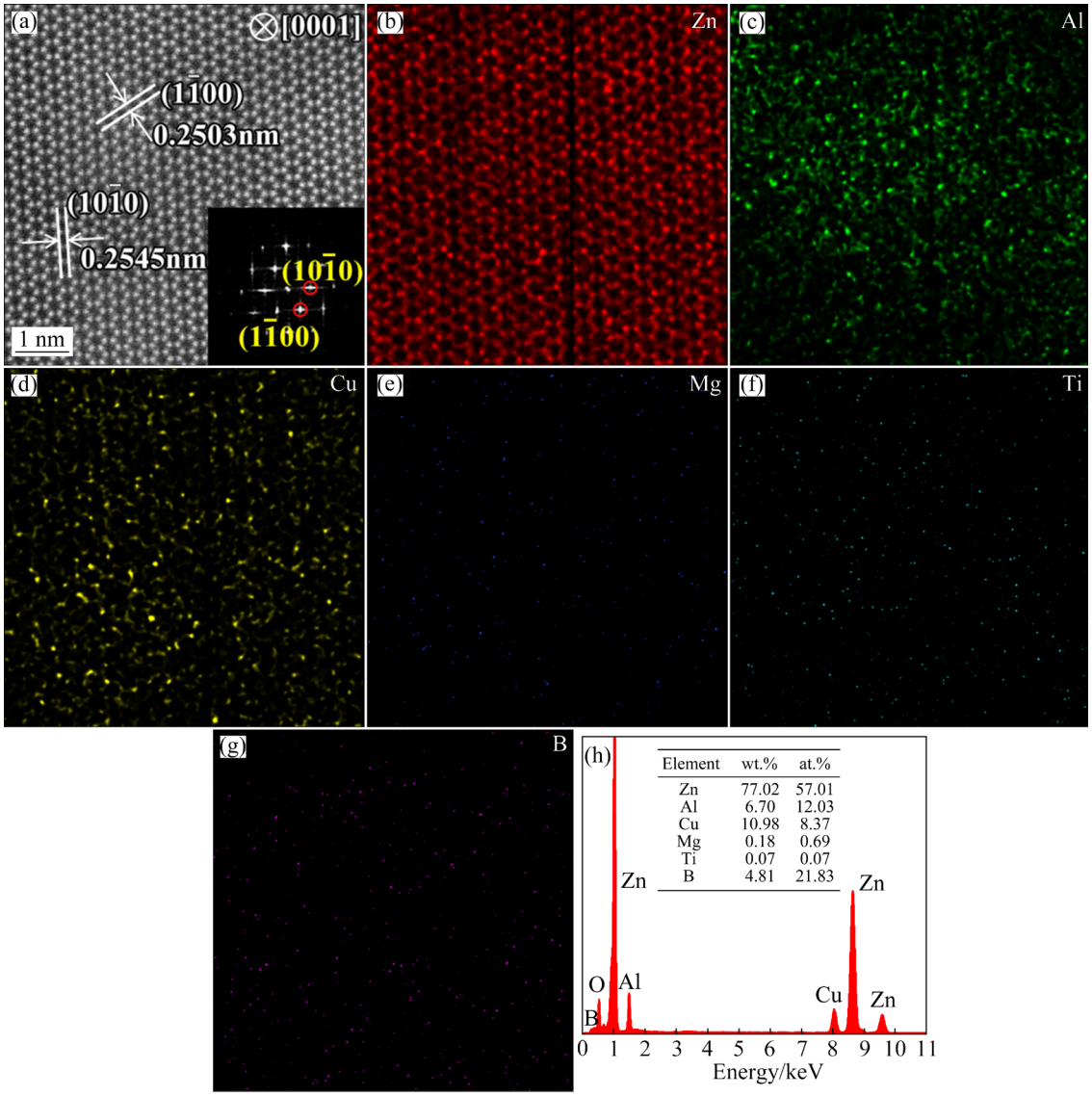

Fig. 15 Atomic-resolution HAADF-STEM image (a) and corresponding EDS mappings (b−g) of η-Zn phase in eutectoid microstructure for as-cast ZA27−0.05(Ti+B) alloy, and EDS results (h) of (a)

primarily Zn, Al, Cu, and B elements with minor amounts of Mg and Ti elements, which is consistent with the results in Figs. 12−14. The precise locations of Al, Cu, Mg, Ti, and B in the η-Zn phase could not yet be identified.

3.2.3 Impact of TiB on primary α(Al) and eutectoid microstructure

According to the obtained results, the addition of modifier not only refined the primary α(Al) phase of the ZA27 alloy but also transformed the coralloid eutectoid microstructure to one that coexists with basket-like and strip-like structures. The refining of the primary α(Al) phase is crucial for improving the mechanical properties of the ZA27 alloy [20]. Additionally, as was already discussed, the basket-like eutectoid microstructure is superior to the coralloid and strip-like eutectoid microstructures in terms of strengthening the alloy. As a result, the modified alloys exhibited better mechanical properties than the unmodified alloy.

The primary α(Al) phase of ZA eutectoid alloys has been reported to be refined by the addition of TiB_2 particles or Al−Ti−B master alloys [18,20,22], but no attention was paid to how this altered the eutectoid microstructure. As a result, the proposed modification mechanisms for the refinement of the primary α(Al) phase were discussed. Due to their significantly higher melting temperatures than those of Al and Zn [28,29], some intermetallic particles, such as TiB_2 and

Al_3Ti [18,20,22], may form first during the solidification of the modified alloys, according to one more widely accepted viewpoint. Due to their favorable lattice matching with α(Al) [20], these particles can act as efficient heterogeneous nucleation sites for α(Al) grains, facilitating the nucleation of the primary α(Al) phase. Another viewpoint claimed that the primary α(Al) phase would be surrounded by hard TiB_2 particles that would act as barriers to grain growth, inhibiting the primary α(Al) phase from growing [18].

However, the modified alloy containing 0.05 wt.% (Ti+B) in this study did not contain TiB_2 and Al_3Ti particles. Therefore, the heterogeneous nucleation and growth retardation do not apply to the primary α(Al) refining explanation of this alloy. The most likely mechanism might be an enrichment of B atoms at the solid−liquid interface, which would lead to constitutional supercooling and prevent the development of primary α(Al) dendrites. The observation of B enrichment in the primary α(Al) can provide evidence in support of this mechanism (Figs. 7(b) and 10(b)). The modification of Zr and Sr on ZA alloys has been explained by a similar mechanism [20,27].

Despite the presence of Al_3Ti particles in the modified alloy with 0.2 wt.% (Ti+B), they do not contribute to the nucleation of primary α(Al). This judgement is supported by the observation that the degree of refinement of the primary α(Al) in the alloy with 0.2 wt.% (Ti+B) was not higher than that in the alloy with 0.05 wt.% (Ti+B). Effectively promoting the nucleation of primary α(Al) is difficult due to the low amounts of the Al_3Ti particles. If considerable amounts of TiB_2 and Al_3Ti particles could be added to the alloy, it could be anticipated that the heterogeneous nucleation and growth retardation mechanisms caused by these particles would also be crucial in the refinement of the primary α(Al). The current work demonstrates that the number of TiB_2 and Al_3Ti particles introduced by suitable additions of Al−5Ti−1B master alloys is constrained. One more effective technique to introduce these particles is the in situ mixed salt route [18].

In addition to refining the primary α(Al) phase, the addition of TiB altered the morphology of the eutectoid microstructure. Our EDS analysis has demonstrated that the eutectoid microstructure had B as well as trace amounts of Ti. The formation of the basket-like and strip-like eutectoid microstructures is suggested to be caused by the involvement of B and/or Ti atoms in the eutectic and eutectoid reactions.

4 Conclusions

(1) Adding TiB modifiers significantly improves the hardness and strength of the as-cast Zn−27Al−2Cu−0.02Mg (wt.%) alloy, but has no impact on its ductility. The maximum Vickers hardness of HV 184 and the maximum tensile strength of 434 MPa are achieved at a (Ti+B) content of 0.05 wt.%.

(2) The addition of TiB refines the primary α(Al) dendritic microstructure and modifies the morphologies of the α(Al) and η-Zn phases in the eutectoid microstructure, though the phase constituents remain unchanged. Ti and B are distributed as solutes in the phase constituents. When more than 0.2 wt.% (Ti+B) is added, part of Ti will exist as Al_3Ti.

(3) The primary α(Al) grains are refined, most likely owing to the enrichment of B atoms at the solid−liquid interface, which may lead to constitutional supercooling and prevent the coarsening of α(Al) dendrites. The modification of the eutectoid microstructure may be related to the involvement of B and/or Ti atoms in the eutectic and eutectoid reactions.

Acknowledgments

This work was supported by the National Natural Science Foundation of China (Nos. 52001119, 51831004, 52171006), and the Fundamental Research Funds for the Central Universities, China.

References

[1] LIU Fu-chu, TU Suo, GONG Xiao-long, LI Guan-jin, JIANG Wen-ming, LIU Xin-wang, FAN Zi-tian. Comparative study on performance and microstructure of composite water-soluble salt core material for manufacturing hollow zinc alloy castings [J]. Materials Chemistry and Physics, 2020, 252: 123257.

[2] XIA Zhao, KONG Gang, ZHANG Shuang-hong, CHE Chun-shan, LAI De-lin. Effect of Mg on the fluidity of zinc alloys [J]. Materials Letters, 2022, 320: 132264.

[3] FUWA D, SAKURAGI T, MIZUBAYASHI M, KOBAYASHI M, KATSUMI T. Prediction of laminations in zinc alloy die-casting by gas−liquid two-phase flow

simulation [J]. Materials Transactions, 2019, 60: 793−801.

[4] GANGWAR S, PAYAK V, PATHAK V K, JAMWAL A, GUPTA P. Characterization of mechanical and tribological properties of graphite and alumina reinforced zinc alloy (ZA-27) hybrid metal matrix composites [J]. Journal of Composite Materials, 2020, 54: 4889−4901.

[5] KHAN M M, DIXIT G. Abrasive wear characteristics of silicon carbide particle reinforced zinc based composite [J]. Silicon, 2018, 10: 1315−1327.

[6] BEDNARCZYK W, WĄTROBA M, KAWAŁKO J, BAŁA P. Can zinc alloys be strengthened by grain refinement? A critical evaluation of the processing of low-alloyed binary zinc alloys using ECAP [J]. Materials Science and Engineering: A, 2019, 748: 357−366.

[7] SAVAŞKAN T, AZAKLI Z, HEKİMOĞLU A P. Effect of heat treatment on mechanical and wear properties of Zn−40Al−2Cu−2Si alloy [J]. Transactions of Nonferrous Metals Society of China, 2021, 31: 2651−2663.

[8] YOUSEFI D, TAGHIABADI R, SHAERI M H. Effect of multi-pass multi-directional forging on tribological properties of Si-rich eutectoid ZA alloys [J]. Transactions of Nonferrous Metals Society of China, 2021, 31: 2024−2038.

[9] POLA A, TOCCI M, GOODWIN F E. Review of micro-structures and properties of zinc alloys [J]. Metals, 2020, 10: 253.

[10] SONG Xiu-an. Study on properties and mechanism of Si-reinforced Zn−Al alloys [J]. Advanced Materials Research, 2011, 328/329/330: 1487−1490.

[11] GANGWAR S, PATNAIK A, YADAV P C, SAHU S, BHAT I K. Development and properties evaluation of marble dust reinforced ZA-27 alloy composites for ball bearing application [J]. Materials Research Express, 2019, 6: 076525.

[12] GANGWAR S, PATNAIK A, BHAT I K. Tribological and thermomechanical analysis of CaO (quicklime) particulates filled ZA-27 alloy composites for bearing application [J]. Proceedings of the Institution of Mechanical Engineers, Part L: Journal of Materials Design and Applications, 2018, 232: 20−34.

[13] MURRAY J L. The Al−Zn (aluminum-zinc) system [J]. Bulletin of Alloy Phase Diagrams, 1983, 4: 55−73.

[14] KUMRUOGLU L C. Prediction of shrinkage ratio of ZA-27 die casting alloy with artificial neural network, computer aided simulation and comparison with experimental studies [J]. Scientia Iranica, 2021, 28: 2684−2700.

[15] ZHANG S Q, CHEN T J, WANG B. Effects of reheating temperature and time on microstructure and tensile properties of thixoformed in situ Sip/ZA27 composites [J]. International Journal of Materials and Product Technology, 2017, 54: 126−146.

[16] ZHANG Hui, ZHU Yan-qing, LI Ning, HUANG Yao, ZHAO Cheng-zhi, ZHANG He-xin. The influence of Mg/Cu on tensile properties of ZA27 alloy [J]. IOP Conference Series: Materials Science and Engineering, 2019, 605: 012015.

[17] LI Ming-yang, LU Shu-jing, LONG Fang, SHENG Meng, GENG Hao-ran, LIU Wen-di. Effect of Y addition on the mechanical properties and microstructure of Zn−Al alloys [J]. JOM, 2015, 67: 922−928.

[18] CHEN Fei, WANG Tong-min, CHEN Zong-ning, MAO Feng, HAN Qiang, CAO Zhi-qiang. Microstructure, mechanical properties and wear behaviour of Zn−Al−Cu−TiB_2 in situ composites [J]. Transactions of Nonferrous Metals Society of China, 2015, 25: 103−111.

[19] CHEN Fei, WANG Bin-bin, CAO Zhi-qiang. Microstructure and wear behavior of in situ ZA27/TiB_2 composites [J]. Metals, 2020, 10: 1663.

[20] LI Nan, LIU Xiao-jing, WANG Qing-zhou, CUI Chun-xiang, YIN Fu-xing, JI Xiang-wei, JIAO Zhi-xian. Effect of combined addition of Al−Ti−B ribbon and Zr element on the microstructure, mechanical and damping properties of ZA22 alloy [J]. Materials & Design, 2017, 127: 97−105.

[21] LIANG S, SCHMID-FETZER R. Thermodynamic assessment of the Al−Cu−Zn system, Part III: Al–Cu–Zn ternary system [J]. Calphad: Computer Coupling of Phase Diagrams and Thermochemistry, 2016, 52: 21−37.

[22] ZHANG Jian-jun, WANG Qing-zhou, JIAO Zhi-xian, CUI Chun-xiang, YIN Fu-xing, YAO Chang. Effects of combined use of inoculation and modification heat treatment on microstructure, damping and mechanical properties of Zn−Al eutectoid alloy [J]. Materials Science and Engineering: A, 2020, 790: 139740.

[23] YIN Mei-jie, CHEN Jiang-hua, WANG Shuang-bao, LIU Zi-ran, CHA Li-mei, DUAN Shi-yun, WU Cui-lan. Anisotropic and temperature-dependent growth mechanism of *S*-phase precipitates in Al−Cu−Mg alloy in relation with GPB zones [J]. Transactions of Nonferrous Metals Society of China, 2016, 26: 1−11.

[24] LAI Yu-xiang, FAN Wei, YIN Mei-jie, WU Cui-lan, CHEN Jiang-hua. Structures and formation mechanisms of dislocation-induced precipitates in relation to the age-hardening responses of Al−Mg−Si alloys [J]. Journal of Materials Science & Technology, 2020, 41: 127−138.

[25] JIAO Ning-ning, LAI Yu-xiang, CHEN Shu-lin, GAO Peng, CHEN Jiang-hua. Atomic-scale roles of Zn element in age-hardened AlMgSiZn alloys [J]. Journal of Materials Science & Technology, 2021, 70: 105−112.

[26] ZHOU Lin, WU Cui-lan, XIE Pan, NIU Feng-jiao, MING Wen-quan, DU Kui, CHEN Jiang-hua. A hidden precipitation scenario of the θ'-phase in Al−Cu alloys [J]. Journal of Materials Science & Technology, 2021, 75: 126−138.

[27] LIU Yang, GENG Cong, ZHU Yun-ke, CHEN Xu. Effect of Sr addition on microstructure evolution and mechanical properties of Zn−4%Al hypoeutectic alloy [J]. Journal of Alloys and Compounds, 2017, 695: 443−451.

[28] LI Bing-hong, LIU Ying, LI Jun, GAO Sheng-ji, CAO Hui, HE Lin. Effect of tungsten addition on the microstructure and tensile properties of in situ TiB_2/Fe composite produced by vacuum induction melting [J]. Materials & Design, 2010, 31: 877−883.

[29] NOFAR M, MADAAH HOSSEINI H R, KOLAGAR-DAROONKOLAIE N. Fabrication of high wear resistant Al/Al_3Ti metal matrix composite by in situ hot press method [J]. Materials & Design, 2009, 30: 280−286.

TiB 的添加对 ZnAl 合金改性的微观影响

周玉琳[1,2]，宋文豪[1]，赖玉香[1]，陈江华[1,3]

1. 湖南大学 材料科学与工程学院 高分辨电镜中心，长沙 410082；
2. 湖南有色金属控股集团有限公司，长沙 410015；
3. 海南大学 皮米电镜中心，海口 570228

摘　要：采用扫描电子显微镜、高角度环形暗场扫描透射电子显微镜和能量 X 射线谱，研究 TiB 的加入对锌铝共晶(ZA27)合金改性的微观作用。铸造一系列 Zn−27Al−2Cu−0.02Mg−x(Ti+B) (x=0，0.01，0.02，0.05，0.10，0.20，质量分数，%)合金。研究结果表明，ZA27 合金的硬度和强度随(Ti+B)含量的增加而提高，在(Ti+B)含量为 0.05%时达到最高值。TiB 改性剂可以细化初生 α(Al)相晶粒，改变珊瑚状(α(Al)+η-Zn)共析组织的微观结构，这是 ZA27 合金力学性能提高的原因。改性后的共析组织表现出篮状和条状共析组织微观结构特点。初生 α(Al)相晶粒的细化很可能与 B 在固−液界面上偏析引起的成分过冷有关。B 和/或 Ti 参与共晶和共析反应，改变了共析组织的形态。

关键词：Zn−Al 合金；TiB 改性剂；显微组织；力学性能；电子显微术

(Edited by Xiang-qun LI)